Eur. Phys. J. D (2017) 71: 64
DOI: 10.1140/epjd/e2017-70408-4

THE EUROPEAN PHYSICAL JOURNAL D

Regular Article

Electronic energy loss of protons and deuterons in multi-walled carbon nanotubes

Carlos E. Celedón[1,2,3,a], Andrea Cortés[4], Esteban A. Sánchez[2,3], M. Sergio Moreno[2,3], Juan David Uribe[1], Nestor R. Arista[2,3], and Jorge E. Valdés[1]

[1] Laboratorio de Colisiones Atómicas, Departamento de Física, Universidad Técnica Federico Santa María, 1680 Valparaíso, Chile
[2] Centro Atómico Bariloche, Av. Exequiel Bustillo 9500, R8402AGP San Carlos de Bariloche, Río Negro, Argentina
[3] Instituto Balseiro, Av. Exequiel Bustillo 9500, R8402AGP San Carlos de Bariloche, Río Negro, Argentina
[4] Departamento de Física, Facultad de Ciencias, Universidad Católica del Norte, 1280 Casilla Antofagasta, Chile

Received 24 June 2016 / Received in final form 21 October 2016
Published online 16 March 2017 – © EDP Sciences, Società Italiana di Fisica, Springer-Verlag 2017

Abstract. Results of measurements of electronic energy loss for few keV protons and deuterons interacting with multi-walled carbon nanotubes are presented. Analyses of the energy loss distributions, for both type of ions, show a particular shape which is due to the cylindrical geometry of the nanotubes. These distributions can be explained in detail by a Monte Carlo simulation program that includes elastic and inelastic processes and the geometrical properties of the nanotubes. The electronic energy loss values obtained from this study are proportional to the ion velocity, but are lower than the corresponding values for amorphous carbon. This indicates that the ion-nanotube interaction is affected by the electronic and crystalline structure of the nanotubes. Comparisons with experimental values for different types of C targets and with recent theoretical calculations were also done.

1 Introduction

In the last decade, multi-wall carbon nanotubes (MWCNTs) have been the subject of great interest due their wide range of potential applications in electronics [1], optical [2], medical [3,4] and biomaterial [5] areas. One aspect of particular interest in this area is to study the interaction of these structures with energetic particles (ions or electrons), either as a method to analyze their properties or to modify them.

Several theoretical studies have been published using dielectric response methods to describe the interaction of swift ions with MWCNTs [6]. From the point of view of these nanotubes structure, many theoretical and experimental studies of irradiation effects on nanotubes by swift ions (light and heavy) have been carried out, in the ranges of high and medium energies [7–10].

By contrast with this, in the range of low energies there are only a few experimental works on energy loss of slow light ions interacting with carbon nanostructures [11,12] where the main contribution to the energy loss is due to the interaction with electrons in the valence and conduction bands.

In this work we measure and analyse the exit energy distribution of protons and deuterons incident perpendicular to the main axis of lying down MWCNTs, in the low-energy range $E_0 < 10$ keV/u. The MWCNTs were self-supported on a TEM grid, and the measurements were performed using the transmission geometry [13]. Additionally, we performed Monte Carlo type computer simulations to analyze the experimental results. From these studies we obtain the mean electronic energy loss (stopping power) of the nanotubes and analyze the dependence of the shape and energy loss spectra with the thickness of the nanotube walls.

2 Experimental

2.1 Sample preparation

Synthesis of alumina templates (AAO) were prepared by anodic oxidation of aluminum foils (of 99.999% purity) in two stages in an oxalic acid electrolyte, at 20 °C, for 4 h, with an applied voltage of 40 V [14,15]. CNTs were grown using a chemical vapor deposition (CVD) method. The proportion of gas precursors used were acetylene/argon (1:20), and the synthesis time of 15 min at 650 °C. After the CVD process, and in order to obtain a CNTs suspension, the template was dissolved with a sodium hydroxide (5% w) solution, washed with deionised water. In order to get the higher amount of single CNTs exposed to the beam, the suspension was diluted several times to reduce their pile-up. Carbon nanotubes were characterized by Transmission Electron Microscopy (TEM) and

[a] e-mail: carlos.celedon@usm.cl

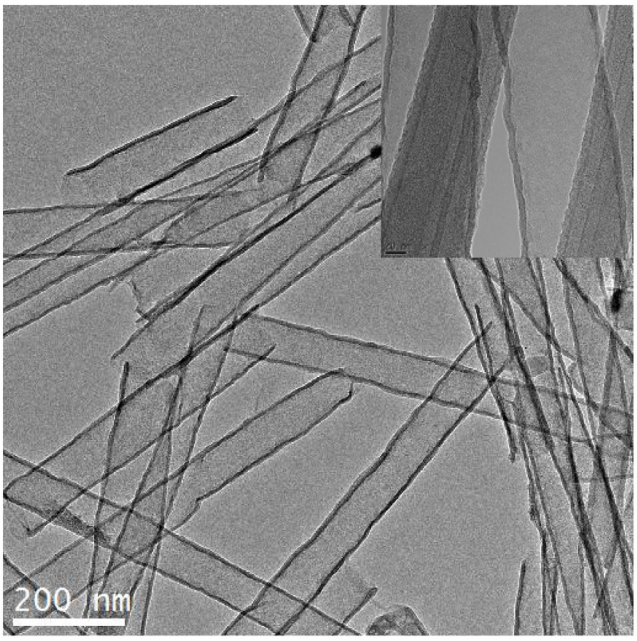

Fig. 1. HRTEM image of multi-wall carbon nanotubes and the inset show details of the wall structure and thickness.

Raman spectroscopy ($\lambda = 532$ nm laser). The tubes were straight with estimated outer diameters of ∼85 nm, see Figure 1, and show the typical signature of metallic multi-walls CNTs [16], as observed in Raman spectroscopy. Figure 1 shows MWCNTs supported on a TEM grid with a pile-up proportion of about 60%, and 40% of just single CNTs exposed to the beam.

2.2 Energy loss measurements

The experiments and energy loss measurements were performed in the Low Energy Accelerator (LEA) laboratory of the Centro Atómico Bariloche, and in the Atomic Collisions Laboratory (LCA) of the Physics Department, Universidad Técnica Federico Santa María. The energy loss measurements with proton and deuteron beams were performed with self supported MWCNT's mounted on gold TEM grids (400 mesh). These grids CNTs without any substrate using the same setting and geometry as described in a previous work [13]. In order to minimize the elastic energy loss and multiple scattering contribution to the energy loss [17,18], the velocity dependence of the stopping power was determined with the detector fixed in the forward direction ($\theta = 0°$). The angular acceptance of the cylindrical analyzer was 0.8°. Figure 2 shows schematically the setup of the present experiment.

3 Computer simulations

3.1 Energy loss model

Following previous studies, the excitation of valence or conduction band electrons of C, can be described by a free electron gas (FEG) model, where the energy loss per unit path length, $S_e = dE/dx$ (electronic stopping power), has dependence proportional to velocity, of the form

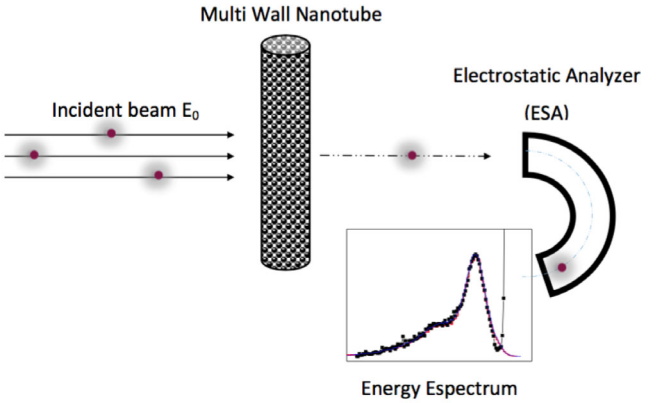

Fig. 2. Schematic experimental setup.

$$S_e = \frac{dE}{dx} = Q(r_s)v \tag{1}$$

where Q is the stopping coefficient, that can be obtained directly from Density Functional Theory (DFT) [19,20] or from Monte Carlo simulations, and r_s is the Wigner-Seitz radius for the electrons, which may be derived from measurements of plasmon frequencies [21]. The electronic stopping power S_e is related to the electronic Stopping Cross Section (SCS) through, $SCS = 1/\eta\, S_e$, where η is the atomic density of the material.

Experimental values of plasmon frequencies for CNTs have been reported in various articles [22–25], showing a dependence of the energy values on the wall thickness of MWCNTs [26]. In this work they conclude that this variation not only depends on the electron density but also on the strength of the screening and in the effective interaction at inter-atomic distances. The correlation between the excitations observed in the CNTs and the wall thickness is not straight forward, but it suggests that also a variation of the stopping coefficient can be found with the characteristic of the MWCNTs.

3.2 Monte Carlo simulation

Monte Carlo (MC) simulations allow to take into account the main physical features of the scattering process, including the properties of the target, stopping forces, fluctuations in the energy loss (intrinsic straggling) and interatomic potentials, in order to analyse and explain the main features of the experiments.

MC simulations of the energy loss as a function of the observation angle have been performed on the classical scattering approach using the binary collision model with a random atom distribution in the solid, similar to those applied in previous works [13,27,28].

A projectile that passes through a material loses part of its initial energy E_0 by collisions with the electrons (inelastic collisions) and with the nuclei (elastic collisions)

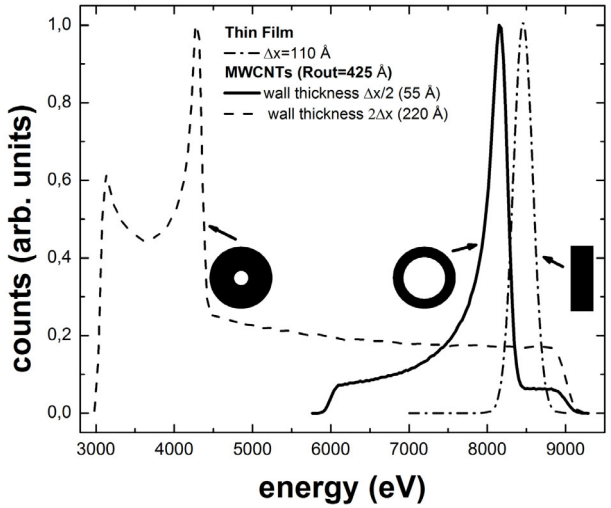

Fig. 3. Shape of the energy loss spectrum obtained from $\Delta E = \eta \cdot SCS \cdot \Delta x$ for thin film target and for carbon nanotubes with different wall thickness.

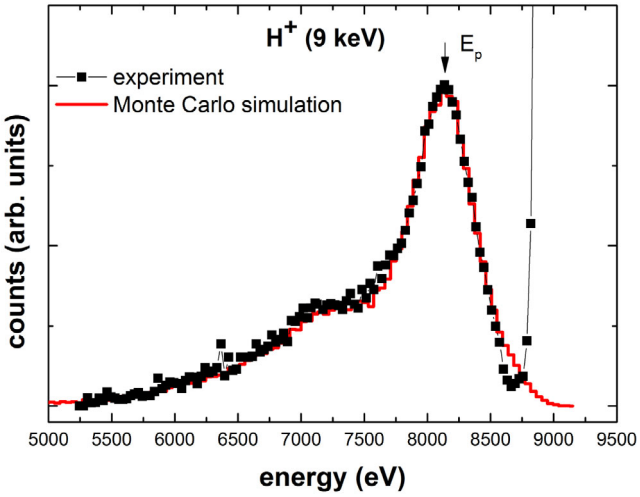

Fig. 4. Energy Loss spectrum of 9 keV protons transmitted across self-supported MWCNT's mounted on a TEM grid. Red solid line shows the results of Monte Carlo simulations with 50% of MWCNT's overlap.

that constitute the solid. For this reason, and in order to perform a description of the process involved in the energy loss and its fluctuations, the modelling requires specific consideration of the physical characteristics and geometric shape of the target material, such as roughness, thickness or radius, among others. The geometry of the target influences the shape of the energy loss distribution. In the case of ion transmission through uniform thin films, the characteristic energy loss distributions show an almost Gaussian shape (see Fig. 3a), while for a cylindrical target geometry the different thicknesses crossed by the projectile generate a singular energy loss distribution formed by an asymmetric peak lying on top of a background, whose shape and relative contributions depend on the radius and thickness of the cylinder (see Figs. 3b and 3c). In order to explain the shape and value of experimental energy loss spectra for projectiles crossing a target with cylindrical geometry we use a Monte Carlo simulation based on classical dynamics approach [13,28].

The parameters required for these simulations were extracted from High Resolution Transmission Electron Microscopy images of the nanotubes (see Fig. 1). With a statistical analysis of these images it was possible to obtain information on inner and outer diameters of the nanotubes. The mean value for inner and outer diameters was $D_{in} = 74$ nm and $D_{out} = 85$ nm and the corresponding standard deviations were 10 nm and 2 nm. The particular geometry of the target precludes obtaining the stopping power by just dividing the main energy loss by the sample thickness, as in a uniform thin foil. In the present case the stopping coefficient was obtained by adjusting the results of the most probable value of the energy loss distribution, E_p, obtained from the Monte Carlo simulations, to the corresponding E_p value of the experimental energy loss distribution, for each experimental measurement, as a function of incident ion energy. The energy binning used in the MC analysis was 12 eV. The systematic error of the deduced values is estimated to be less than 10%.

Due to the statistical nature of the collision processes, usually described as energy loss straggling [12,13], a normal Gaussian distribution function was used to model the intrinsic fluctuations of this energy loss.

In order to describe the interaction between the projectile and target, the Moliére interatomic potential was used with the usual Lindhard screening length [29,30].

Finally, the energy loss distribution obtained from the MC simulations were convoluted with the experimentally measured dispersion characteristic of the electrostatic analyzer.

4 Results and discussion

Figures 4–7 show some experimental energy loss spectra of protons and deuterons with energies $E_0 = 9$ keV and 6 keV measured in the forward direction ($\theta = 0°$), transmitted across the MWCNTs. The energy loss spectra obtained from these CNT's show two overlapping peaks, and peculiar differences in the shape of the energy loss distributions, as compared with the energy loss spectra of protons crossing a thin carbon film, which typically have a simple Gaussian function shape [30].

Analysis of Monte Carlo results, obtained by varying the geometry of the carbon-nanotubes, confirms that these shape differences in the energy loss distributions are due to the different geometries and to the existence of hollow regions which depend on the wall thickness. Nanotubes with equal wall thicknesses but different external diameters, have similar values for the most probable energy loss (within 1%), but show differences in the total widths of the energy loss distribution. For nanotubes with the same diameters and different wall thicknesses, with increasing nominal wall thickness, the spectrum of energy loss broadens and the energy losses shift to lower values (see Fig. 3).

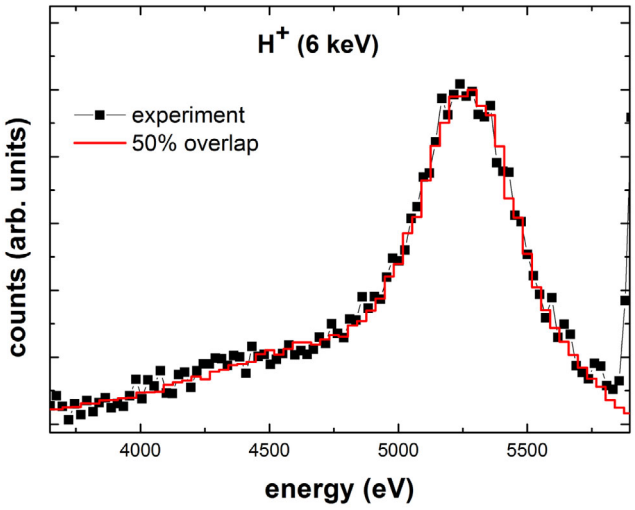

Fig. 5. Energy Loss spectrum of 6 keV protons transmitted across self-supported MWCNT's mounted on a TEM grid. Red solid line shows the results of Monte Carlo simulations with 50% of MWCNT's overlap.

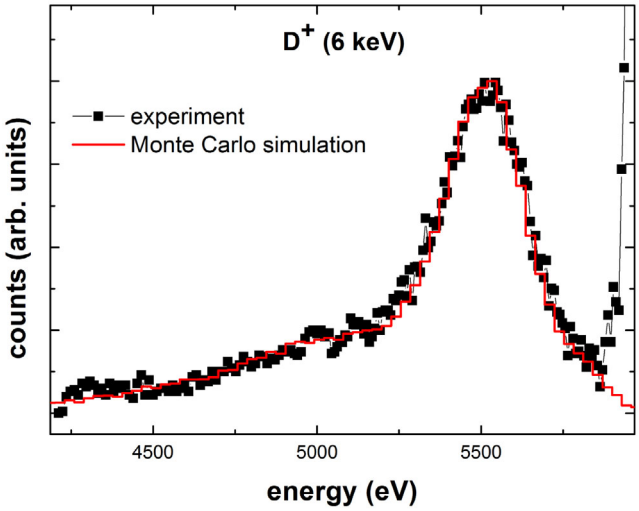

Fig. 7. Energy Loss spectrum of 6 keV deuterons transmitted across self-supported MWCNT's mounted on a TEM grid. Red solid line shows the results of Monte Carlo simulations with 50% of MWCNT's overlap.

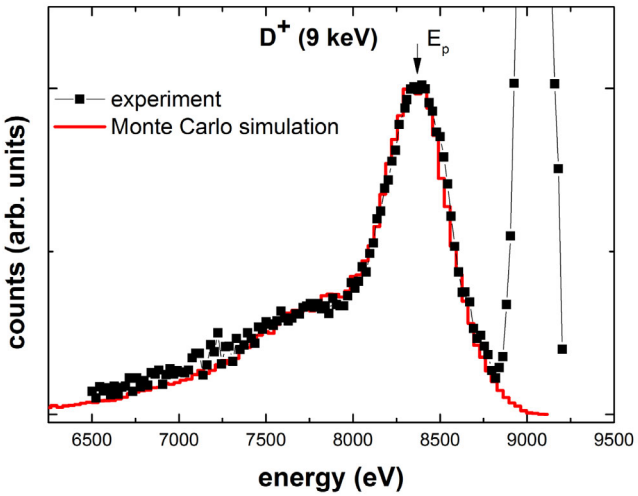

Fig. 6. Energy Loss spectrum of 9 keV deuterons transmitted across self-supported MWCNT's mounted on a TEM grid. Red solid line shows the results of Monte Carlo simulations with 50% of MWCNT's overlap.

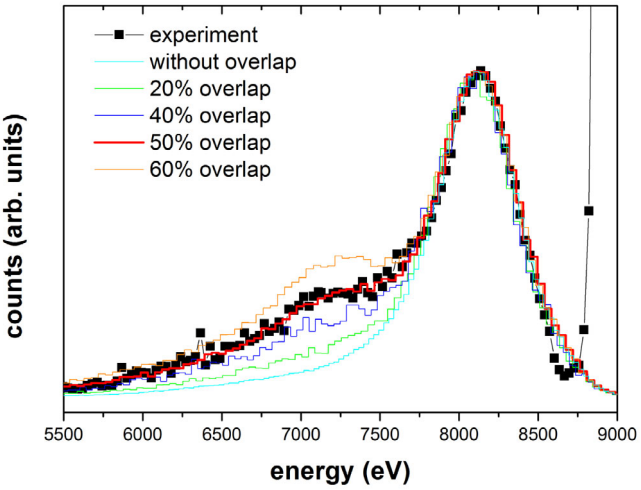

Fig. 8. Energy Loss spectrum of 9 keV protons transmitted across self-supported MWCNT's mounted on a TEM grid. Color lines shows the energy loss spectrum for different overlap percentage of MWCNT's.

Similar analyses of Monte Carlo simulations show that the peculiar shape of the energy loss spectra, consisting of a main peak and high-energy shoulder, is produced by the contribution of the overlapping of MWCNTs deposited on TEM grids, which in fact can be observed in Figure 1.

In Figure 8, we show the results of the simulations for different percentages of overlap of MWCNTs, between 20 and 60%. This overlap modifies the shoulder observed at lower outgoing projectile energies, producing larger energy losses, and is caused by the increase of the sample thickness in the superposition. The intensity of this shoulder increases with the percentage of CNTs overlap. The best agreement with the experimental energy loss spectrum is obtained with a 50% overlap of the CNTs, that it is consistent with the pile-up observed in Figure 1. In this analysis we have considered the overlap ot two NTs. As seen in Figure 1, most of the overlaps correspond to two MWCNTs, so that no multiple overlaps have been considered. Multiple overlaps would contribute to the very low energy part of the energy distribution, thus not afecting the stopping power determination.

To explain the main peak and the strong asymmetry in the energy loss spectrum we separated in the MC simulation the spectrum corresponding to those particles incident on the central region of the nanotube (with impact parameters $y < R_{in}$) and to those incident on the outer region ($y > R_{in}$). The result is shown by the different curves in Figure 9. Thus, we clearly observed that the

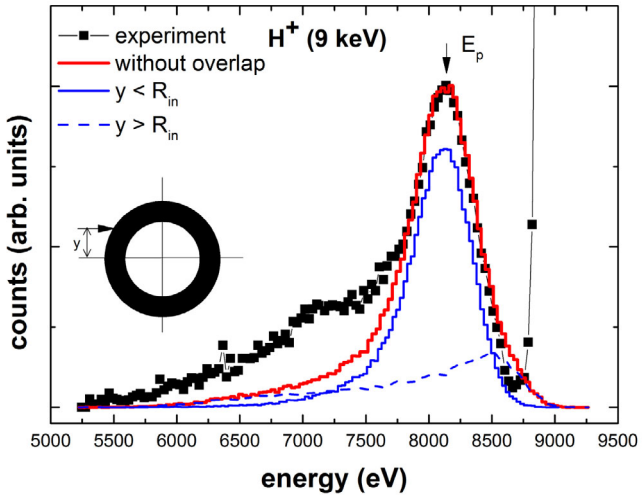

Fig. 9. Energy loss spectrum of 9 keV protons transmitted across MWCNT's self-supported on a TEM grid. Red solid line shows the results of Monte Carlo simulations without MWCNT's overlap. The blue lines show the distributions corresponding to impact parameters in the central region ($y < R_i n$) and the external regions ($y > R_i n$) of the nanotube, as described in the text. Main contribution to the energy loss spectrum comes from the central part of the nanotube.

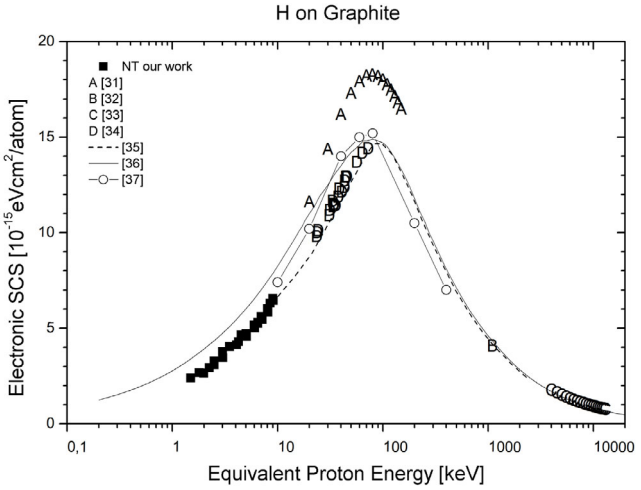

Fig. 10. Comparison of the electronic stopping cross section for hydrogenic ions in graphite and in MWCNT's, as a function of the equivalent proton energy. The squares show our experimental data. Open circles from Ref. [31] corresponding to TD-DFT calculations of SCS of graphitic targets. Letter symbols are experimental values from references [32–35]. The lines correspond to calculations performed for protons with SEICS code [36], and the semi-empirical compilation SRIM 2003 [37].

strong peak at $E = E_p$ corresponds to particles crossing the central region which is the thinnest part of the nanotube. By contrast, those particles crossing the rim of the NT produce a long tail in the energy loss spectrum. Additionally, we show in this figure the contribution to the spectrum produced by the overlapping of nanotubes, which produces a wide distribution of energy losses in the intermediate region of the energy loss spectrum.

In Figure 10 we present for comparison a collection of data obtained for the electronic SCS as a function of the proton energy [31–37]. To determine the SCS values from energy loss measurements we used the atomic density $\eta_{graphite} = 1.12 \times 10^{23}$ at/cm^3. Experimental values for carbon type targets [32–35] and a semi-empirical curve from the SRIM code [37] are shown. Additionally, we show calculations performed with the SEICS code [36] and from first principle using time dependent density functional theory for graphitic targets [31]. The data obtained in the present experiment for H^+ and D^+ are plotted with black circles and squares, respectively. Our results agree fairly well with most of the previous measurements and calculations, and extend the experimental data to projectile energies lower than 10 keV.

In Figure 11 we show the MWCNTs SCS obtained for protons and deuterons as a function of the equivalent proton velocity, together with amorphous carbon SCS values in the energy range below 10 keV from [30,38–40]. Also shown in this plot is the value from DFT [20]. According to these first principles calculations and our experimental fitted values with Monte Carlo simulations, the obtained stopping values (Eq. (1)), are described with $r_s = 2.1$. This value corresponds to 2 electrons per C atom, considering the atomic density of graphite, which indicates that

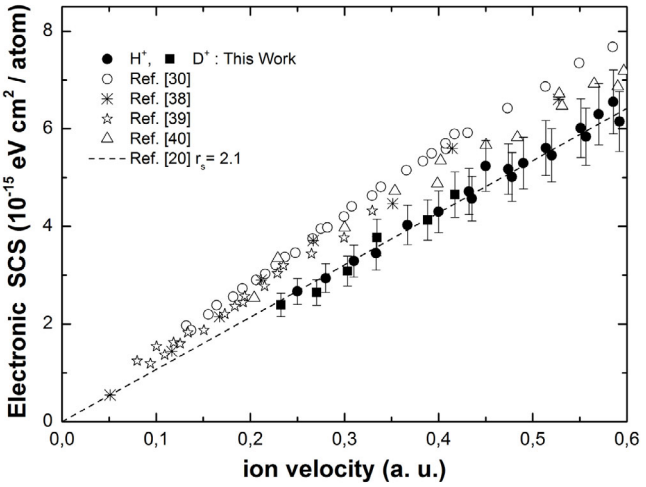

Fig. 11. Electronic stopping cross section for hydrogenic ions in MWCNT's, as a function of the projectile velocity. The full-circles (H^+) and full-squares (D^+) show our experimental data and other symbols correspond to carbon SCS for protons obtained in previous experiments in amorphous targets [30,38–40]. The dashed line shows the values obtained from the DFT calculations [20].

on average the ions sample regions of lower densities in the crystalline target. We notice also, that this r_s value is larger than that of amorphous carbon $r_s = 1.66$ and graphite $r_s = 1.53$ [21]. This indicates that the electronic density sampled by the protons is lower than the mean density for those materials.

5 Conclusions

We have measured the energy loss of protons and deuterons in the low-energy range ($E_0 < 10$ keV) traversing self supported MWCNTs.

The shapes of the energy loss spectra show asymmetries and striking differences from those obtained from carbon foils, and a particular dependence with the thickness of the carbon nanotubes, which reveals interesting differences arising from the peculiar geometries of these nanostructures.

We have been able to explain in great detail the shapes of the energy loss spectra of MWCNTs by computer simulations which include elastic and inelastic interactions and energy loss straggling effects.

The MC simulation permits to separate the contributions to the energy loss spectra due to particles crossing different regions of the NTs, as well as the effect produced by statistical overlapping of nanotubes.

Results of electronic energy loss for H^+ and D^+ transmitted across MWCNTs, observed in the forward direction, show a proportional velocity dependence of the mean energy loss in the range of low energies. No evidence of threshold effects (observed in other materials [41–45]) is observed here, indicating a simple metallic-like behavior of the stopping power. Additionally, our experimental data are lower than the corresponding values for amorphous carbon. This result poses interesting questions both for experimental and theoretical research. On one side, it would be of interest to perform similar experiments with MWCNT's of different radii to test a possible dependence of the SCS with the number of walls of the nanotubes (similar to the already observed dependence of plasmon energies with the number of walls mentioned before). On the other hand, on the theoretical side the present results call for ab initio calculations of stopping coefficients considering the particular geometry of MWCNT's, similar perhaps to those already performed for graphene targets [31,46].

The stopping coefficient in MWCNTs, can be described by the standard DFT [20] assuming a jellium model with a Wigner-Seiz radius $r_s = 2.1$. This value corresponds to a contribution of 2 electrons per carbon atom to the electronic stopping process.

In summary, the experimental results reported here, together with the computer simulations and theoretical analysis, provide novel information and a consistent description of the phenomenon of the interaction of low-energy ions with multi-wall carbon nanotubes. We expect that the results of this study will stimulate alternative experiments with focused electron or ion beams in several energy ranges, and will be useful for the spectroscopic analysis of nano-structures.

This work has been financially supported by the following grants: Fondecyt 1100759 – Conicyt – Chile and ANPCYT of Argentina. Also, acknowledges to UTFSM-DGIP, CEDENNA and ANILLO ACT1204 grants.

Author Contribution statement

C.C. and J.E.V designed the project and directed it with help from A.C., who prepare nanotubes samples and M.S.M. provide microscopy characterisation of nanotubes. C.C., J.D.U. and E.A.S. performed measurements and carried out data analyses. N.R.A. provided theoretical support. All authors contributed to discussions and participate in the manuscript writing.

References

1. D.Y. Lee, C.Y. Shin, S.J. Yoon, H.Y. Lee, W. Lee, N.K. Shrestha, J.K. Lee, S.H. Han, Sci. Rep. **4**, 3930 (2014)
2. E.V. Santiago, S.H. López, M.A. Camacho López, D.R. Contreras, R. Farías-Mancilla, S.G. Flores-Gallardo, Opt. Laser Technol. **84**, 53 (2016)
3. C.P. Firme, P.R. Bandaru, Nanomedicine **6**, 245 (2010)
4. H. He, L.A. Pham-Huy, P. Dramou, D. Xiao, P. Zuo, C. Pham-Huy, Biomed Res. Int. **2013**, 578290 (2013)
5. S. Pramanik, R. Konwarh, N. Barua, A.K. Buragohain, N. Karak, Biomater. Sci. **2**, 192 (2014)
6. Z.L. Mišković, J. Phys. Conf. Ser. **133**, 012011 (2008)
7. W.K. Hong, C. Lee, D. Nepal, K.E. Geckeler, K. Shin, T. Lee, Nanotechnology **17**, 5675 (2006)
8. B. Khare, M. Meyyappan, M.H. Moore, P. Wilhite, H. Imanaka, B. Chen, Nano Lett. **3**, 643 (2003)
9. V.A. Basiuk, K. Kobayashi, T. Kaneko, Y. Negishi, E.V. Basiuk, J.M. Saniger-Blesa, Nano Lett. **2**, 789 (2002)
10. P.J. Boul, K. Turner, J. Li, M.X. Pulikkathara, R.C. Dwivedi, E.D. Sosa, Y. Lu, O.V. Kuznetsov, P. Moloney, R. Wilkins, M.J. O'Rourke, V.N. Khabashesku, S. Arepalli, L. Yowell, J. Phys. Chem. C **113**, 14467 (2009)
11. A.V. Krasheninnikov, F. Banhart, Nat. Mater. **6**, 723 (2007)
12. J.E. Valdés, C. Celedón, R. Segura, I. Abril, R. Garcia-Molina, C.D. Denton, N.R. Arista, P. Vargas, Carbon **52**, 137 (2013)
13. C. Celedón, E.A. Sánchez, M.S. Moreno, N.R. Arista, J.D. Uribe, M. Mery, J.E. Valdés, P. Vargas, Phys. Rev. A **88**, 012903 (2013)
14. R. Lavin, J.C. Denardin, J. Escrig, D. Altbir, A. Cortes, H. Gomez, J. Appl. Phys. **106**, 103903 (2009)
15. A. Cortés, R. Lavín, J.C. Denardin, R.E. Marotti, E.A. Dalchiele, P. Valdivia, H. Gómez, J. Nanosci. Nanotechnol. **11**, 3899 (2011)
16. D.K. Singh, P. Iyer, P. Giri, Diam. Relat. Mater. **19**, 1281 (2010)
17. J. Eckardt, G. Lantschner, M. Jakas, V. Ponce, Nucl. Instrum. Methods Phys. Res. B **2**, 168 (1984)
18. J.E. Valdés, G. Tamayo, G. Lantschner, J. Eckardt, N. Arista, Nucl. Instrum. Methods Phys. Res. B **73**, 313 (1993)
19. P. Echenique, R. Nieminen, R. Ritchie, Solid State Commun. **37**, 779 (1981)
20. M. Puska, R. Nieminen, Phys. Rev. B **27**, 6121 (1983)
21. D. Isaacson, *Compilation of r_s values* (Tech. rep., New York University, 1975)
22. P.M. Ajayan, S. Iijima, T. Ichihashi, Phys. Rev. B **47**, 6859 (1993)

23. L.A. Bursill, P.A. Stadelmann, J.L. Peng, S. Prawer, Phys. Rev. B **49**, 2882 (1994)
24. M. Kociak, L. Henrard, O. Stéphan, K. Suenaga, C. Colliex, Phys. Rev. B **61**, 13936 (2000)
25. A. Seepujak, U. Bangert, A.J. Harvey, P.M.F.J. Costa, M.L.H. Green, Phys. Rev. B **74**, 075402 (2006)
26. M. Upton, R. Klie, J. Hill, T. Gog, D. Casa, W. Ku, Y. Zhu, M. Sfeir, J. Misewich, G. Eres, D. Lowndes, Carbon **47**, 162 (2009)
27. W. Möller, G. Pospiech, G. Schrieder, Nucl. Instrum. Methods **130**, 265 (1975)
28. M. Famá, J. Eckardt, G. Lantschner, N. Arista, Phys. Rev. A **62**, 062901 (2000)
29. M. Nastasi, J.W. Mayer, J.K. Hirvonen, *Ion-Solid Interactions* (Cambridge University Press, 1996)
30. E.D. Cantero, G.H. Lantschner, N.R. Arista, Eur. Phys. J. D **65**, 397 (2011)
31. A. Ojanperä, A.V. Krasheninnikov, M. Puska, Phys. Rev. B **89**, 035120 (2014)
32. J.D. Pearce, J. Appl. Phys. **52**, 5056 (1981)
33. S.D. Softky, Phys. Rev. **123**, 1685 (1961)
34. N. Sakamoto, H. Ogawa, N. Shiomi-Tsuda, Nucl. Instrum. Methods Phys. Res. B **115**, 84 (1996)
35. W. Käferböck, W. Rössler, V. Necas, P. Bauer, M. Peñalba, E. Zarate, A. Arnau, Phys. Rev. B **55**, 13275 (1997)
36. P. de Vera, I. Abril, R. Garcia-Molina, Appl. Radiat. Isot. **83**, 122 (2014)
37. J.F. Ziegler, Nucl. Instrum. Methods Phys. Res. B **219-220**, 1027 (2004)
38. E.P. Arkipov, Y.V. Gott, Soviet Phys. J. Exp. Theor. Phys. **29**, 614 (1969)
39. S.H. Overbury, P.F. Dittner, S. Datz, R.S. Thoe, Radiat. Eff. Defects Solids **41**, 219 (1979)
40. H.H. Andersen, A. Csete, T. Ichioka, H. Knudsen, S.P. Møller, U.I. Uggerhøj, Nucl. Instrum. Methods Phys. Res. B **194**, 217 (2002)
41. J.E. Valdés, G. Tamayo, G. Lantschner, J. Eckardt, N. Arista, Nucl. Instrum. Methods Phys. Res. B **73**, 313 (1993)
42. E. Cantero, G. Lantschner, J. Eckardt, N. Arista, Phys. Rev. A **80**, 032904 (2009)
43. S. Markin, D. Primetzhofer, M. Spitz, P. Bauer, Phys. Rev. B **80**, 205105 (2009)
44. D. Goebl, D. Roth, P. Bauer, Phys. Rev. A **062903**, 1 (2013)
45. C.E. Celedón, E.A. Sánchez, L. Salazar Alarcón, J. Guimpel, A. Cortés, P. Vargas, Nucl. Instrum. Methods Phys. Res. B **360**, 103 (2015)
46. S. Bubin, B. Wang, S. Pantelides, K. Varga, Phys. Rev. B **85**, 235435 (2012)